Pairing symmetries of a hole-doped extended two-orbital model for the pnictides

Andrew Nicholson,[1,2] Weihao Ge,[1,2] José Riera,[3] Maria Daghofer,[4] Adriana Moreo,[1,2] and Elbio Dagotto[1,2]
[1]*Department of Physics and Astronomy, University of Tennessee, Knoxville, Tennessee 37996, USA*
[2]*Materials Science and Technology Division, Oak Ridge National Laboratory, Oak Ridge, Tennessee 37831, USA*
[3]*Instituto de Física Rosario, Universidad Nacional de Rosario, 2000-Rosario, Argentina*
[4]*IFW Dresden, P.O. Box 27 01 16, DE-01171 Dresden, Germany*
(Received 3 November 2011; revised manuscript received 10 January 2012; published 24 January 2012)

The hole-doped ground state of a recently introduced extended "t-U-J" two-orbital Hubbard model for the Fe-based superconductors is studied via exact diagonalization methods on small clusters. Similarly as in the previously studied case of electron doping [A. Nicholson *et al.*, Phys. Rev. Lett. **106**, 217002 (2011)], upon hole doping it is observed that there are several competing pairing symmetries, including A_{1g}, B_{1g}, and B_{2g}. However, contrary to the electron-doped case, the ground state of the hole-doped state has pseudocrystal momentum $\mathbf{k} = (\pi,\pi)$ in the unfolded Brillouin zone. In the two Fe-atom per unit cell representation, this indicates that the ground state involves antibonding, rather than bonding, combinations of the orbitals of the two Fe atoms in the unit cell. The lowest state with $\mathbf{k} = (0,0)$ has only a slightly higher energy. These results indicate that this simple two-orbital model may be useful to capture some subtle aspects of the hole-doped pnictides, since calculations for the five-orbital model have unveiled a hole pocket centered at M [$\mathbf{k} = (\pi,\pi)$] in the unfolded Brillouin zone.

DOI: 10.1103/PhysRevB.85.024532 PACS number(s): 74.20.Rp, 71.10.Fd, 74.70.Xa, 75.10.Lp

I. INTRODUCTION

The detailed study of the recently discovered high critical temperature superconductivity (HTCS) in the iron-based pnictides and chalcogenides[1] continues providing important information to understand the still puzzling mechanism that drives this remarkable phenomenon. Experiments indicate that these Fe-based materials share many properties with the high-T_c cuprates,[2] such as magnetically ordered parent compounds[3] and superconducting states stabilized by either electron or hole doping.[1] However, there are also remarkable differences, such as the fact that the parent compounds, at least for the pnictides, are (bad) metals rather than Mott insulators. Moreover, several of the iron d orbitals are active at the Fermi surface (FS) as opposed to the case of the cuprates, where just the copper $d_{x^2-y^2}$ orbital plays the major role. While it has been clearly established that the superconducting pairing operator has d-wave symmetry in the case of the hole-doped cuprates,[4] the symmetry of the pairing operator in the pnictides is still controversial: surface-sensitive angle-resolved photoemission (ARPES) studies[5] indicate that full nearly-momentum-independent gaps open on all FS pockets, compatible with the $s_{\pm}$ state.[6] However, several other experiments testing bulk properties provide results compatible with nodal superconductivity.[7]

Reliable theoretical studies are difficult to implement for the complex multiorbital models needed for these materials without making explicit assumptions about the ground-state properties or about the mechanism and strength of the pairing interactions. Under the assumption of a magnetically driven superconducting instability, the random-phase approximation (RPA) is often applied in this context, providing indications that several pairing channels, mostly A_{1g} and B_{1g}, are in competition in this type of compounds.[8] However, RPA relies on a particular subset of Feynman diagrams and it is a weak-coupling approach. On the opposite extreme, strong-coupling studies have also been performed. Depending on the particular model used, some authors have found evidence of pairing with B_{2g} symmetry,[9] while others have found a variety of competing states.[10] A complementary approach to these previous investigations is to perform an exact diagonalization (ED) of the model Hamiltonians, allowing us to solve the problem exactly for any value of the interaction. However, since the Hilbert space grows exponentially with the system size, this method can be implemented only in very small clusters and with a reduced number of active Fe orbitals. This ED approach has been recently applied by the authors and collaborators to the study of an electron-doped two-orbital Hubbard model, and in that effort the presence of competing pairing states was observed as the strength of the coupling parameters was varied.[11–13]

An important characteristic of the widely studied Hubbard models for the pnictides/chalcogenides is that they are not particle-hole symmetric. On the experimental side, superconductivity has been found both upon electron and hole doping, but it seems that hole-doped materials belonging to the 122 family are more suitable for the use of surface-sensitive techniques, while electron-doped materials belonging to the 1111 family are more easily studied with bulk techniques.[5,7] Then, it is natural to wonder whether a potential source of the differences in the experimental results regarding the pairing symmetries may arise from the nature of the dopants. For this reason it is important to study theoretically the properties of multiorbital Hubbard models under both electron and hole doping. Previously, such a comparative analysis has been performed employing the RPA method applied to a five-orbital Hubbard model.[14] For the parameter range studied in that case (weak coupling), a pairing state with A_{1g} symmetry was observed in both cases. The state found has nodes on the electron pockets in the electron-doped case, but upon hole doping an extra hole pocket at the $M = (\pi,\pi)$ point in the Brillouin zone leads to the removal of the nodes and the development of a nodeless $s_{\pm}$ state.[14]

The goal of the present publication is to study the most favorable pairing channels of a two-orbital Hubbard model

using small-cluster exact diagonalization techniques (namely, the Lanczos algorithm) for the case of hole doping and to contrast the results against those found for the case of electron doping of the same model that have been recently reported.[11–13] To reduce the severe constraints imposed by the small size of the clusters that can be diagonalized in present day computers, a simple generalization of the Hubbard model for the pnictides, previously introduced for the study of the electron-doped case,[11] will be here applied. For this purpose, Heisenberg "J" terms will be added to the original Hubbard model to enhance spin order and pairing tendencies, but without projecting out doubly occupied sites and charge fluctuations. These terms help to establish tightly bound states upon doping that can be studied with Lanczos methods on the small clusters currently accessible with state-of-the-art computers. Comparisons with RPA results for the five-orbital model and with experimental data will be performed.

The organization of the paper is as follows: the model and the method are reviewed in Sec. II, the main results for hole doping are presented in Sec. III, while Sec. IV is devoted to the conclusions.

II. MODEL AND METHOD

The model studied here is based on the well-known and widely used two-orbital Hubbard model[12,13,15] that employs the d_{xz} (x) and d_{yz} (y) Fe orbitals. These orbitals provide the largest contribution to the pnictides' band structure at the FS.[16] The reduction in the actual number of active orbitals in the pnictides is necessary in order to perform the present Lanczos studies. Calculations with more orbitals for the same cluster studied here are simply not possible at present.

The parameters of the electronic hopping terms of the model were previously chosen to provide a close agreement with the band-structure calculations obtained with density-functional theory.[15] In addition to the hopping terms, the model also includes the on-site Coulomb interaction consisting of intra- and interorbital Coulomb repulsions with couplings U and U', the Hund's rule coupling $J_{\rm H}$, and the pair-hopping term with strength J'. While U can in principle depend on the particular orbital due to different screening effects for each orbital, this is not the case for the d_{xz} and d_{yz} orbitals that form a degenerate e_g doublet, implying that the relations $U' = U - 2J_{\rm H}$ and $J' = J_{\rm H}$ are fulfilled for symmetry reasons.[17] This Hamiltonian, with the kinetic-energy hopping and onsite-interaction terms mentioned above, has been studied in detail previously.[12,13,15,18] Moreover, in a recent investigation of the electron-doped case,[11] the model was supplemented by Heisenberg interactions to amplify the strength of the magnetic state and, consequently, the pairing strength as well.

Naively, it may seem that selecting a stronger on-site Hubbard interaction would stabilize a stronger antiferromagnetic state. However, this procedure also induces an insulator, and actually the strength of the effective coupling between the Fe spins decreases as $1/U$ with increasing U. To avoid this problem, in early studies of the one-band t-U-J model[19] and in a recent study of the electron-doped two-orbital model,[11] Heisenberg terms have been added and shown to enhance pairing tendencies. Since our aim is to investigate the symmetries of the Cooper pairs, the additional magnetic interactions must have the same symmetries as the original Hamiltonian. To make sure that the symmetries are properly handled, the additional Heisenberg interaction is given by the operatorial form that corresponds to the superexchange terms derived from the strong-coupling (large-U) limit. In the case of the one-band Hubbard model, this is a Heisenberg term with spin $S = 1/2$. In the case of a multiorbital model away from half filling, the corresponding superexchange contains an orbital degree of freedom in addition to the spin, and it is of a Kugel-Khomskii type.[20,21]

In the present case of a half-filled two-orbital model, the low-energy Hilbert space for the strong-coupling limit, with both U and $J_{\rm H}$ large, is given by doubly occupied sites with singly occupied orbitals. Due to the Hund's coupling, the two electrons per site form a triplet state, with an energy $E_0 = U' - J_{\rm H} = U - 3J_{\rm H}$, compared to $E_1 = U' + J_{\rm H} = U - J' = E_0 + 2J_{\rm H}$ and $E_2 = U + J_{\rm H} = E_0 + 4J_{\rm H}$ for inter- and intraorbital singlet states. The low-energy Hilbert space is, thus, given by a spin $S = 1$ at each site. The interaction between these spins can be obtained by second-order perturbation theory in an analogous manner as the well-known derivation of the Heisenberg model from the one-orbital Hubbard model. The calculation for the two orbitals is most easily carried out when the hopping term preserves orbital flavor, because the first hopping process, which creates a virtual excitation with energy $U + J_{\rm H}$, then has to involve the same orbital as the second, which goes back to the low-energy Hilbert subspace. By this procedure it can be shown that the result is the isotropic Heisenberg interaction for $S = 1$ with a coupling

$$J_{\rm eff} = \frac{2}{3}\frac{t_a^2 + t_b^2}{U + J_{\rm H}}, \tag{1}$$

where t_a and t_b are the hopping parameters corresponding to the two orbitals. With the notation $t_{a/b} = t_{1/2}$,[15] the nearest-neighbor (NN) coupling $J_{\rm NN}$ can be derived. For a next-nearest-neighbor (NNN) coupling, which is natural since in the original Hubbard model the hoppings involve both NN and NNN Fe atoms, it is convenient to transform to a rotated orbital basis $(|xz\rangle \pm |yz\rangle)/\sqrt{2}$, where the hoppings are diagonal in orbital space and given by $t_3 \pm t_4$, leading to

$$J_{\rm NNN} = \frac{4}{3}\frac{t_3^2 + t_4^2}{U + J_{\rm H}} = 2\frac{t_3^2 + t_4^2}{t_1^2 + t_2^2} J_{\rm NN}. \tag{2}$$

Similarly as in the previous investigation of Ref. 11 and to avoid the proliferation of parameters, the ratio $J_{\rm NNN}/J_{\rm NN}$ is kept fixed to 0.93, which is the value that results from $t_1 = -1$, $t_2 = 1.3$, $t_3 = t_4 = -0.85$.[15] For the electron-doped case, the results were found to be not sensitive to changes in this ratio as long as the model remains in the regime with $(\pi,0)/(0,\pi)$ magnetic order.[11]

The extended two-orbital Hubbard Hamiltonian is exactly investigated using the Lanczos algorithm[2,22] on a tilted $\sqrt{8} \times \sqrt{8}$ cluster, as done in previous studies.[2,12,13] In spite of the small size of the cluster, this still requires substantial computational resources. More specifically, even exploiting

the Hamiltonian symmetries the calculation of the undoped-limit ground state of the eight-site cluster still requires a basis with ∼2–20M states (slightly more demanding than a 16-site cluster one-band Hubbard model), depending on the subspace explored. Runs applying the Lanczos technique had to be performed for all the allowed momenta $\mathbf{k}$ of the cluster, for all the quantum numbers under rotations and reflections (i.e., all the irreducible representations A_{1g}, A_{2g}, B_{1g}, B_{2g}, and E_g of the D_{4h} symmetry group[13]), and also for all the z-axis total spin projections. In addition, the computation of binding energies for the case of hole doping requires calculations for a number of electrons N equal to 14, 15, and 16, varying U, $J_{\rm H}$, and $J_{\rm NN}$ using a fine grid. For these reasons, the overall effort amounted to ∼8000 diagonalizations of the cluster, supplemented also by calculations of dynamical properties, using a Penguin 128GB Altus 3600 computer.

III. RESULTS

It is important to remind the readers that the most commonly used models for the pnictides are usually defined in the so-called unfolded Brillouin zone.[8,13,15,23,24] Due to the symmetry of the Fe-As planes,[15,23] it is possible to describe the pnictides using Fe-only effective models where the As atoms merely provide a bridge for the electronic hopping between the irons. Under this approximation only one Fe atom is left per unit cell to describe these materials.[25] As a result of these considerations, the number of orbitals to be considered is reduced by half, which is a computational advantage, and the size of the Brillouin zone (BZ) is doubled. For this reason, the momentum in the unfolded zone is dubbed "pseudocrystal" momentum.[23] In order to relate the model results to experiments addressing the BZ corresponding to two Fe atoms, it is necessary to "fold" the extended BZ in such a way that the pseudocrystal momentum $\mathbf{k}=(\pi,\pi)$ is folded onto momentum (0,0). The physical difference between states with $\mathbf{k}=(0,0)$ and (π,π) is that the first indicates a bonding and the second an antibonding combination of the d orbitals in the two Fe atoms in the two-atom unit cell. In the presentation of our results below, $\mathbf{k}$ will stand for pseudocrystal momentum.

A. Phase diagram

The relative symmetry between the undoped ($N=16$) ground state (GS) and the $N=14$ GS has been studied with the Lanczos technique varying $U/|t_1|$ and $J_{\rm H}/U$. The undoped GS was found to have momentum $\mathbf{k}=(0,0)$, and it transforms according to the A_{1g} representation of the D_{4h} group, for all the values of $J_{\rm H}$ and U studied here, in agreement with previous results.[13] However, a surprising result found in the present study of the hole-doped extended two-orbital model is the presence of many competing low-energy states not only with different symmetries as in the electron-doped case[11] but also with different pseudocrystal momenta $\mathbf{k}$. In other words, low-lying states with both $\mathbf{k}=(0,0)$ and (π,π) were found in our Lanczos investigation. This is compatible with previous mean-field approximation results that also reported low-energy spin-singlet pair states with momentum (π,π).[26]

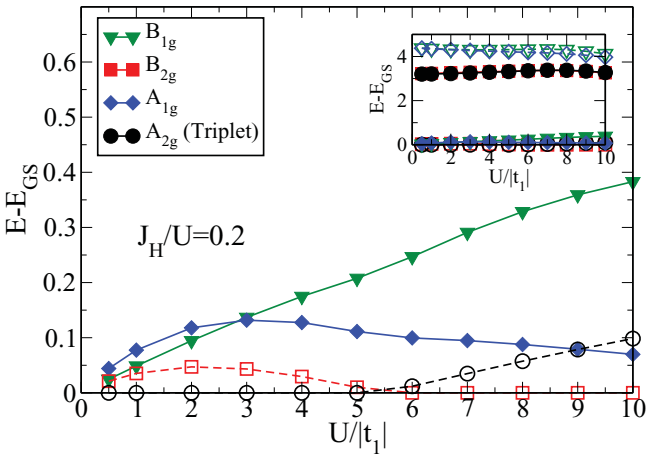

FIG. 1. (Color online) Difference between the energy of the lowest excited state with the symmetry and momentum indicated and the ground state. Full (open) symbols denote $\mathbf{k}=(0,0)$ [$\mathbf{k}=(\pi,\pi)$]. The results are obtained using the Lanczos algorithm for the two-orbital model in an eight-site cluster with 14 electrons (two holes doping), varying the Hubbard repulsion U, and at a fixed $J_{\rm H}/U=0.20$. The inset shows a larger energy range in which the lowest lying state with each symmetry is displayed. The results shown in this figure are without the extra $J_{\rm NN}$ and $J_{\rm NNN}$ terms.

The competition among low-lying states with different symmetries and with different values of $\mathbf{k}$ is presented in Fig. 1 for the case $J_{\rm H}/U=0.20$, without the extra "J" terms. Numerically, it was found that the ground state for 14 electrons has crystal momentum (π,π). For small values of U this state is a triplet with A_{2g} symmetry (open circles in the figure). With increasing U, a transition (via a level crossing) occurs at $U\sim 6|t_1|$ to a spin-singlet ground state with B_{2g} symmetry (open squares in the figure). However, it can be observed that there are states with $\mathbf{k}=(0,0)$ that have very similar energies. For example, for this pseudocrystal momentum, and in the weak-coupling regime, a spin-singlet state with B_{1g} symmetry (represented with filled triangles in the figure) is the closest in energy to the ground state, while for $U\geqslant 3|t_1|$ a spin-singlet state with A_{1g} symmetry prevails (represented with filled diamonds in the figure).

Similar results were found for all the values of U and $J_{\rm H}$ studied; i.e., the $N=14$ ground state has total momentum $\mathbf{k}=(\pi,\pi)$ but there are $\mathbf{k}=(0,0)$ states close in energy with a different symmetry. For this reason, the phase diagrams obtained by varying $J_{\rm H}/U$ and $U/|t_1|$ for *both* values of the pseudocrystal momentum will be presented.

The relative symmetry between the ground state with two electrons less than half filling with total pseudocrystal momentum $\mathbf{k}=(0,0)$ and the undoped ground state is shown in Fig. 2(a), varying $J_{\rm H}/U$ and $U/|t_1|$. A region with symmetry B_{1g}, indicated by the triangles, is found for small $U/|t_1|$ (roughly $U/|t_1|\leqslant 3$) and moderate to large values of $J_{\rm H}/U$. For larger values of $U/|t_1|$, the symmetry changes to A_{1g}. A similar transition from B_{1g} to A_{1g} (extended s wave) has been found using the RPA technique for an electron-doped five-orbital model at $J_{\rm H}=0$.[8] The binding energy $E_{\rm B}$, defined as $E_{\rm B}=E(14)+E(16)-2E(15)$, where $E(N)$ is the GS energy for N electrons, was also calculated. It was found that

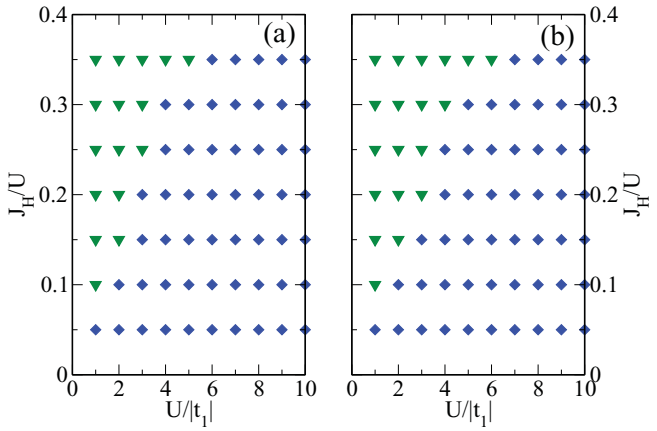

FIG. 2. (Color online) Relative symmetry between the $N = 16$ (undoped) and $N = 14$ [with $\mathbf{k} = (0,0)$] ground states, varying U and J_H/U. Triangles denote B_{1g}-symmetric singlets and diamonds denote A_{1g}-symmetric singlets. (a) Results for couplings $J_{NN} = J_{NNN} = 0$. (b) Results for the lowest value of (J_{NN}, J_{NNN}) where binding appears with a fixed ratio $J_{NN}/J_{NNN} = 0.93$.[11]

without the addition of Heisenberg terms there are no regions with binding.

For the other case of a pseudocrystal momentum $\mathbf{k} = (\pi,\pi)$, the analogous numerical results are shown in Fig. 3(a). It was found that an A_{2g} spin-triplet ground state, indicated by circles in the figure, dominates for large values of J_H/U and small $U/|t_1|$. For the electron-doped model, an A_{2g} spin triplet with momentum (0,0) was similarly observed at large J_H and small U.[12,13] For smaller J_H/U and larger $U/|t_1|$, a spin-singlet ground state with B_{2g} symmetry is the ground state. For this pseudocrystal momentum, the binding energy was calculated as well: binding was obtained for $J_H/U = 0.35$ where a spin-triplet ground state with symmetry A_{2g} prevails (see open triangles in the figure).

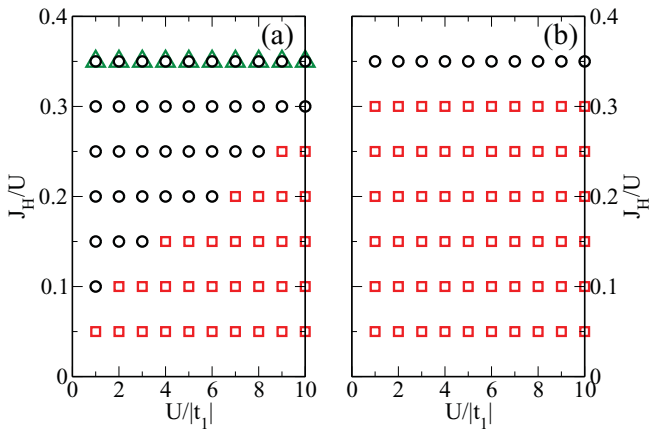

FIG. 3. (Color online) Relative symmetry between the $N = 16$ (undoped) and $N = 14$ [with $\mathbf{k} = (\pi,\pi)$] ground states varying U and J_H/U. Circles denote spin-triplet states and squares denote B_{2g}-symmetric singlets. (a) Results for couplings $J_{NN} = J_{NNN} = 0$. Open triangles indicate binding. (b) Results for the lowest value of (J_{NN}, J_{NNN}) where binding appears with a fixed ratio $J_{NN}/J_{NNN} = 0.93$.[11]

B. Binding stabilization

To stabilize hole binding in the two-orbital model, we will proceed as in the previous investigation of the electron-doped case[11] by adding extra Heisenberg terms, namely a NN coupling J_{NN} and a NNN coupling J_{NNN} as discussed in Sec. II. As in the electron-doped case, and as already explained, J_{NN} will be varied while J_{NN}/J_{NNN} will be kept fixed at the value 0.93.[11]

The results for pseudocrystal momentum $\mathbf{k} = (0,0)$ are presented in Fig. 2(b), showing the symmetry of the hole-doped ground state for the lowest value of J_{NN} where binding of holes is achieved. The phase diagram remains largely unchanged by the addition of the Heisenberg terms except for the B_{1g} region that has expanded slightly towards larger values of U. On the other hand, for states with momentum $\mathbf{k} = (\pi,\pi)$ the spin-triplet region virtually disappears [Fig. 3(b)], except for those triplet states that already had $E_B < 0$ at $J_{NN} = 0$, leaving behind a much larger B_{2g} region in parameter space.

In Fig. 4(a), the binding energy E_B *vs*. J_{NN}/U for states with momentum $\mathbf{k} = (0,0)$ is shown for several values of U and at a fixed (realistic) $J_H/U = 0.2$. Increasing J_{NN} eventually induces binding for all U's. The value of J_{NN}/U where binding occurs decreases as U increases. Figure 5(a) shows the same information but for the states with momentum $\mathbf{k} = (\pi,\pi)$, where a similar qualitative behavior is observed.

A study of the binding energy E_B and the relative symmetry between the $N = 16$ and 14 GS's allows us to construct phase diagrams in the $(U, J_{NN}/U)$ plane. In Fig. 4(b), typical results for the case $J_H/U = 0.2$ are shown[27] for the states with total momentum $\mathbf{k} = (0,0)$. The bound state has A_{1g} symmetry in most of the binding region, but a state with B_{1g} symmetry prevails at smaller U values ($\sim 3|t_1|$). In Fig. 5(b) the same information is displayed but for states with total momentum $\mathbf{k} = (\pi,\pi)$. In this case, the entire binding region,

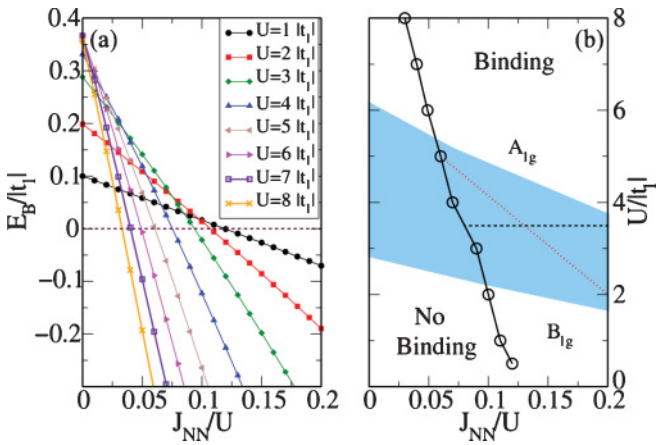

FIG. 4. (Color online) Results for states with total momentum $\mathbf{k} = (0,0)$. (a) $E_B/|t_1|$ vs J_{NN}/U for different values of $U/|t_1|$, at $J_H/U = 0.2$ and $J_{NN}/J_{NNN} = 0.93$. (b) Phase diagram showing "binding" and "no binding" regions and the symmetry of the two-hole bound state varying $U/|t_1|$ and J_{NN}/U, at a fixed $J_H/U = 0.2$. The shaded area indicates the so-called physical region obtained from standard mean-field calculations that were compared with neutrons, transport, and photoemission experimental results.[28] The dotted line is for Fig. 7 (a).

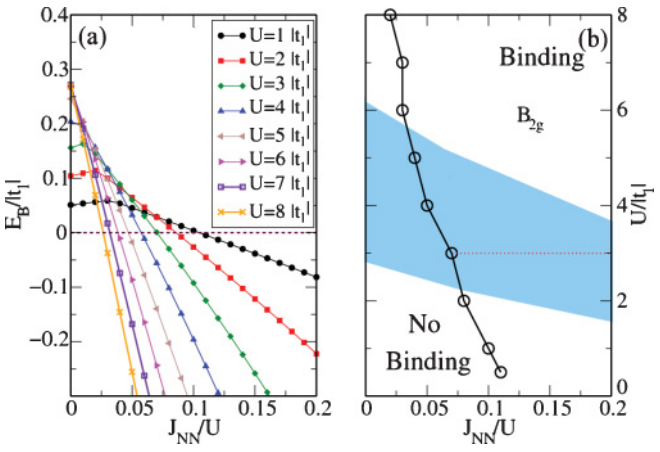

FIG. 5. (Color online) Results for states with total momentum $\mathbf{k} = (\pi,\pi)$. (a) $E_B/|t_1|$ vs J_{NN}/U for different values of $U/|t_1|$, at $J_H/U = 0.2$ and $J_{NN}/J_{NNN} = 0.93$. (b) Phase diagram showing "binding" and "no binding" regions and the symmetry of the two-hole bound state varying $U/|t_1|$ and J_{NN}/U, at a fixed $J_H/U = 0.2$. The shaded region indicates the "physical region" according to standard mean-field calculations.[28] The dotted line is for Fig. 7(b).

except for $J_H/U > 0.3$, has B_{2g} symmetry. All of the above symmetries appear inside the proper magnetic/metallic region of the undoped limit (indicated with shading in the figures) that were obtained in previous mean-field calculations[18,28] extended to incorporate J_{NN}.[11]

C. Magnetism

Since the two-orbital Hubbard model for the pnictides is not particle-hole symmetric, it is interesting to study how the nature of the doping, namely electrons versus holes, affects the intensity of the magnetic order. In the actual materials, experimental results have shown that the in-plane resistivity of electron and hole-doped FeAs-based pnictides displays a larger anisotropy in the electron-doped case.[29] Thus, it has been conjectured that the xz/yz magnetism is stronger in the electron-doped case, while in the hole-doped case it is weaker with a growing contribution of the xy orbital, disregarded in the two-orbital model, that forms the hole pocket around M.[29] A similar conclusion was reached via the FLEX approximation for the case of electron and hole doping of a five-orbital Hubbard model.[30]

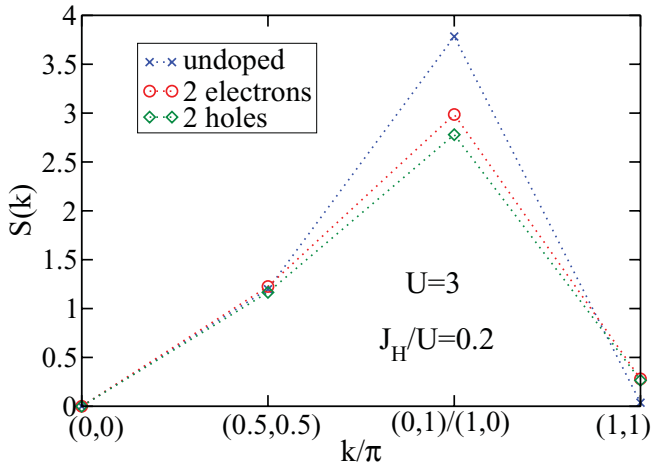

FIG. 6. (Color online) Numerically calculated magnetic structure factor $S(\mathbf{k})$, as a function of the momentum, using an eight-site cluster. Results for the undoped $N = 16$, electron-doped $N = 18$, and hole-doped $N = 14$ cases are indicated, for couplings $U/|t_1| = 3$, $J_H/U = 0.2$, and $J_{NN}/U = 0.2$.

The results for the two-orbital model studied here are shown in Fig. 6, where the magnetic structure factor $S(\mathbf{k})$ is shown in the undoped (crosses), electron-doped (circles), and hole-doped (diamonds) regimes, at fixed couplings $U = 3$, $J_H/U = 0.2$, and $J_{NN}/U = 0.2$, namely, in the mean-field calculated "physical region" indicated in Fig. 5(b). While doping reduces the strength of the peak at $\mathbf{k} = (\pi,0)$, it is interesting to notice that the intensity is slightly more reduced in the hole-doped case. These results lend qualitative support to the notion that the magnetism in the xz and yz orbitals is stronger in the electron-doped case, and it becomes reduced when holes are introduced.

D. Overlap integrals

In this subsection, the functional forms of the hole pairing operators that produce the hole bound states will be analyzed. With this goal, the overlap defined by

$$\langle \Psi_{(N=14)}(\mathbf{k}')|\Delta_{\mathbf{k}'-\mathbf{k},i}|\Psi_{(N=16)}[\mathbf{k} = (0,0)]\rangle \tag{3}$$

was calculated using the Lanczos algorithm along the paths indicated by the dotted lines in the phase diagrams shown in Figs. 4(b) and 5(b). Notice that for $|\Psi_{14}(\mathbf{k}')\rangle$ the pseudocrystal momentum $\mathbf{k}'$ will take the values $(0,0)$ and (π,π) and, thus, a pairing operator with the appropriate $\mathbf{k}' - \mathbf{k}$ has to be used to ensure a nonzero overlap. The ground state $|\Psi(N)\rangle$ in the subspace of N electrons was used, and the operator in Eq. (3) was defined as

$$\Delta_{\mathbf{k},i} = \sum_{\alpha\beta} f(\mathbf{k})(\sigma_i)_{\alpha\beta} d_{\mathbf{k},\alpha,\uparrow} d_{\mathbf{k},\beta,\downarrow}, \tag{4}$$

where $d_{\mathbf{k},\alpha,\sigma}$ destroys an electron with spin z-axis projection σ, at orbital $\alpha = x,y$, and with momentum $\mathbf{k}$. The structure factor $f(\mathbf{k})$ arises from the spatial location of the fermions forming the pair,[13] and σ_i are the Pauli matrices ($i = 1,2,3$) or the 2×2 identity matrix σ_0 ($i = 0$). Note that σ_1 and σ_2 imply an interorbital pairing. Overlaps for all the symmetries in Ref. 13, and with NN and NNN locations for the electronic pairs, were numerically evaluated.

In Fig. 7(a), the overlaps for pairing operators with pseudocrystal momentum $\mathbf{k} = (0,0)$ are presented for values of U and J_H along the dotted path in Fig. 4(b). In the A_{1g} region in Fig. 7(a), we found that the same four pairing operators that have a finite overlap in the electron-doped case[11] also have one here. However, the relative strength of the overlaps differ. For consistency, we will use the same labeling for the operators as in Ref. 11. The A_{1g} operator with the largest overlap is the operator (ii), i.e., the $s_\pm$ operator characterized by $f(\mathbf{k})\sigma_i = (\cos k_x \cos k_y)\sigma_0$, as in the electron-doped case;[11] it is indicated by hollow diamonds in Fig. 7(a). However, in the hole-doped system the overlap for the pairing operator (iv) characterized by $(\cos k_x - \cos k_y)\sigma_3$ (hollow circles) follows in strength; this operator had the

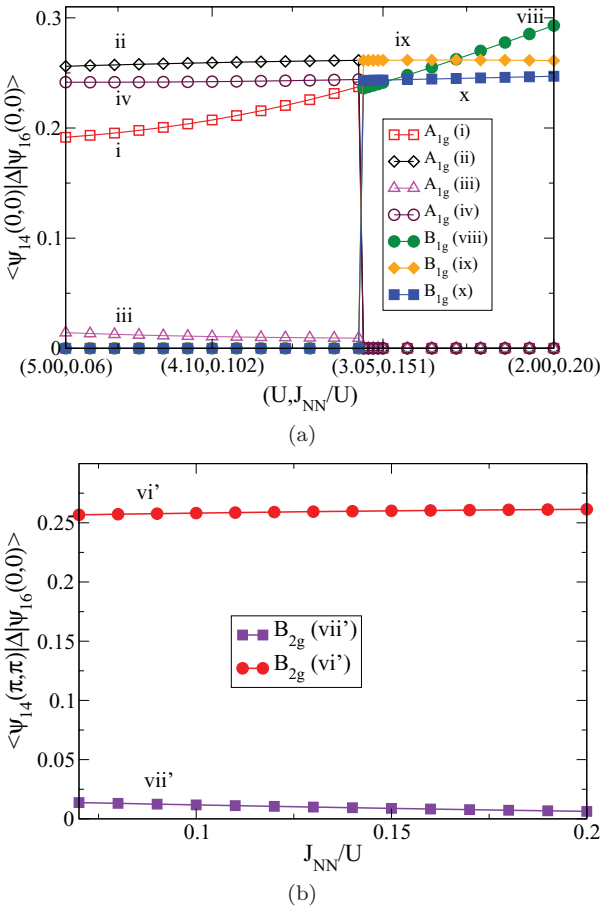

FIG. 7. (Color online) Overlap $\langle\Psi(N=14)|\Delta_{\mathbf{k},i}|\Psi(N=16)\rangle$ vs $J_{\rm NN}/U$ for the indicated pairing operators, at $U=3\,|t_1|$ and $J_{\rm H}/U=0.2$, for (a) states with total momentum $\mathbf{k}=(0,0)$ along the dotted path in Fig. 4(b) and (b) states with total momentum $\mathbf{k}=(\pi,\pi)$ along the dotted path in Fig. 5(b).

weakest overlap in the electron-doped case.[11] The pairing operator (i) with $(\cos k_x+\cos k_y)\sigma_0$ (hollow squares) has an overlap almost as strong as in the electron-doped case. Finally, the overlap corresponding to the operator (iii) $(\sin k_x \sin k_y)\sigma_1$ (hollow triangles) is even more suppressed upon hole doping than upon electron doping.

In the region where the pairs have B_{1g} symmetry there are three pairing operators with large overlaps: (viii) $(\cos k_x+\cos k_y)\sigma_3$ (solid circles), (ix) $(\cos k_x \cos k_y)\sigma_3$ (solid diamonds), and (x) $(\cos k_x-\cos k_y)\sigma_0$ (solid squares). At small values of $J_{\rm NN}/U$, (ix) has the largest overlap amplitude followed by (x) and (viii). However, as $J_{\rm NN}/U$ increases (viii) overtakes (ix).

For the case of pairing operators with pseudocrystal momentum $\mathbf{k}=(\pi,\pi)$, there is one contribution that clearly dominates [see Fig. 7(b)]: (vi') $(\cos k_x \cos k_y)\sigma_1$, which corresponds to a NNN pair with B_{2g} symmetry. The prime in the label is used to remind the reader that the operator has a different pseudocrystal momentum from the B_{2g} state with the same label discussed in the electron-doped case.[11] The only other nonzero pairing overlap occurs for (vii') $(\sin k_x \sin k_y)\sigma_0$ and has a much smaller amplitude than (vi'). Interestingly, the nearest-neighbor B_{2g} operator (v) characterized by $(\cos k_x+\cos k_y)\sigma_1$ that had the strongest overlap in the electron-doped case[11] has zero overlap in the case studied in this manuscript. All the gaps for the pairing operators with B_{2g} symmetry have nodes along the x and y axes.

E. Dynamical pair susceptibilities

To complete our analysis, the dynamical pair susceptibilities defined as

$$P(\omega)=\int_{-\infty}^{\infty} dt e^{i\omega t}\langle\Delta^{\dagger}_{\mathbf{k},i}(t)\Delta_{\mathbf{k},i}(0)\rangle \qquad (5)$$

were also studied in the state with $N=16$ for the pairing operators $\Delta_{\mathbf{k},i}$ introduced in Sec. III D. Notice that the calculated spectral decomposition involves excited states with $N=14$. The procedure described in Ref. 31 in the context of the cuprates will be followed. As discussed above, for $N=14$ there are several low-energy states near the ground state that have different symmetries. The dynamical pair susceptibilities show that most of these low-lying states have a large overlap with $\Delta_{\mathbf{k},i}|\Psi_{\rm N=16}(0)\rangle$ for $\Delta_{\mathbf{k},i}$ with the appropriate symmetry. In Fig. 8, results for $U=3|t_1|$, $J_{\rm H}/U=0.2$, and $J_{\rm NN}/U=0.10$ are presented. Large overlaps with low-lying $N=14$ states are observed for operators (ii) and (iv) with A_{1g} symmetry and (viii) and (x) with B_{1g} symmetry, as well as for operator (vi') with B_{2g} symmetry and pseudocrystal momentum $\mathbf{k}=(\pi,\pi)$.

It is interesting to compare the results obtained for the dynamical pair susceptibility upon hole doping with those obtained for electron doping.[11] In both cases, large susceptibilities for the low-lying states with A_{1g}, B_{1g}, and B_{2g} symmetries are found. This is remarkably different from the case of models for the cuprates where an analogous low-lying overlap analysis showed that $d_{x^2\text{-}y^2}$-wave symmetry clearly dominates over all others.[31]

Returning to pnictides, a similarity between the electron- and hole-doped cases is that the B_{1g} pairing operator that has the highest susceptibility, state (viii), is different from the B_{1g}

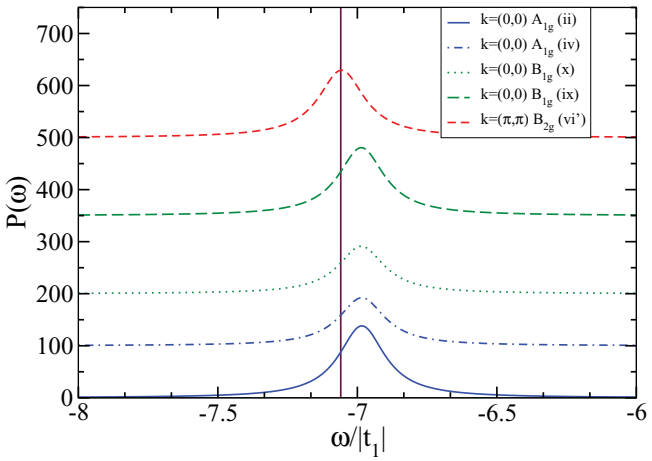

FIG. 8. (Color online) Dynamic pairing susceptibility for the pairing operators with total momentum $\mathbf{k}=(\pi,\pi)$ (operators with B_{2g} symmetry) and with total momentum $\mathbf{k}=(0,0)$ (operators with B_{1g} and A_{1g} symmetry) (see text), at $U=3.0\,|t_1|$, $J_{\rm H}/U=0.2$, and $J_{\rm NN}/U=0.10$. The vertical line indicates $E_{\rm GS}(14)-E_{\rm GS}(16)$.

pairing state for the cuprates. It corresponds to Cooper pairs mainly located on NNN sites, as opposed to the dominant NN contribution in the cuprates, and in the orbital basis used here the B_{1g} symmetry is realized by the orbital degree of freedom. In addition, the susceptibilities indicate that while NN pairs are favored in the electron-doped case NNN have larger susceptibilities upon hole doping for A_{1g} and B_{2g} symmetries.

IV. CONCLUSIONS

The properties of a recently introduced two-orbital extended Hubbard model for the pnictides have been studied upon hole doping with the help of the Lanczos method. The results were contrasted with the previously studied electron-doped case.[11,13] Due to the lack of particle-hole symmetry in the Hamiltonian, the results, as expected, are quantitatively different in both cases. However, an additional surprising characteristic of the hole-doped ground state is that it has pseudocrystal momentum (π,π). In the reduced Brillouin-zone representation corresponding to the physical two Fe-atom per unit cell description of the pnictides, having a nonzero pseudocrystal momentum means that the ground state is characterized by antibonding rather than bonding combinations of the orbitals of the two Fe atoms in the unit cell. In terms of the pairing operators that are favored, it means that the pairs would arise from hole carriers located at the hole pockets centered at Γ and at M in the unfolded Brillouin zone. Interestingly, the five-orbital model for the pnictides[14] shows that upon hole doping a hole pocket, absent in the electron-doped case, develops around M, and this pocket plays an important role in the properties of the hole-doped materials.[14,30] Our results may indicate that a simple toy model, such as the two-orbital model, could be used to study the role that a hole pocket at M plays when multiorbital Hubbard models are hole doped.

In spite of this difference in the pseudocrystal momentum quantum number, there are several commonalities between the hole- and electron-doped two-orbital Hubbard models. The most important feature is that there are several low-lying states with different symmetries close to the undoped ground state. For this reason, the symmetry of the doped states is strongly dependent on the actual values of the interaction parameters. Spin-singlet states that transform according to the irreducible representations A_{1g}, B_{1g}, and B_{2g} were obtained both for hole and for electron doping.

It is remarkable that some of these exact diagonalization results are compatible with the conclusions obtained via approximate studies of more realistic five-orbital Hamiltonians. For example, RPA calculations in the weak-coupling limit[32] indicate that the s- or d-wave symmetry of the pairing operator depends on the crystal structure of the material and the degree and type of doping. Similar results were obtained via a FLEX approximation.[33] An analogous transition from s- to d-wave symmetry was found upon doping using a functional renormalization group approach[34] and also in studies in the strong coupling limit.[10]

The richness of the phase diagrams unveiled here, and in the cited previous investigations, suggests that the symmetry of the pairing state in the pnictides is likely to depend on details of the material under study, as well as on the type of doped carriers (electrons or holes) and on the density of dopants.

ACKNOWLEDGMENTS

This work was supported by the US Department of Energy, Office of Basic Energy Sciences, Materials Sciences and Engineering Division, and also by the National Science Foundation under Grant No. DMR-11-04386 (A. N., W. G., A. M., E. D.), CONICET, Argentina (J. R.), and by the Deutsche Forschungsgemeinschaft under the Emmy-Noether program (M. D.).

[1] For a recent review, see D. C. Johnston, Adv. Phys. **59**, 803 (2010).
[2] E. Dagotto, Rev. Mod. Phys. **66**, 763 (1994).
[3] C. de la Cruz *et al.*, Nature (London) **453**, 899 (2008).
[4] C. C. Tsuei, J. R. Kirtley, C. C. Chi, LockSeeYu-Jahnes, A. Gupta, T. Shaw, J. Z. Sun, and M. B. Ketchen, Phys. Rev. Lett. **73**, 593 (1994).
[5] See for instance T. Kondo *et al.*, Phys. Rev. Lett. **101**, 147003 (2008); H. Ding *et al.*, Europhys. Lett. **83**, 47001 (2008).
[6] I. I. Mazin, D. J. Singh, M. D. Johannes, and M. H. Du, Phys. Rev. Lett. **101**, 057003 (2008); K. Kuroki, S. Onari, R. Arita, H. Usui, Y. Tanaka, H. Kontani, and H. Aoki, *ibid.* **101**, 087004 (2008).
[7] See for instance H.-J. Grafe *et al.*, Phys. Rev. Lett. **101**, 047003 (2008); J. K. Dong, S. Y. Zhou, T. Y. Guan, H. Zhang, Y. F. Dai, X. Qiu, X. F. Wang, Y. He, X. H. Chen, and S. Y. Li, *ibid.* **104**, 087005 (2010).
[8] S. Graser, T. A. Maier, P. J. Hirschfeld, and D. J. Scalapino, New J. Phys. **11**, 025016 (2009).
[9] Q. Si and E. Abrahams, Phys. Rev. Lett. **101**, 076401 (2008).
[10] K. Seo, B. A. Bernevig, and J. Hu, Phys. Rev. Lett. **101**, 206404 (2008).
[11] A. Nicholson, W. Ge, X. Zhang, J. Riera, M. Daghofer, A. M. Oleś, G. B. Martins, A. Moreo, and E. Dagotto, Phys. Rev. Lett. **106**, 217002 (2011).
[12] M. Daghofer, A. Moreo, J. A. Riera, E. Arrigoni, D. J. Scalapino, and E. Dagotto, Phys. Rev. Lett. **101**, 237004 (2008).
[13] A. Moreo, M. Daghofer, J. A. Riera, and E. Dagotto, Phys. Rev. B **79**, 134502 (2009).
[14] A. F. Kemper, T. A. Maier, S. Graser, H-P. Cheng, P. J. Hirschfeld, and D. J. Scalapino, New J. Phys. **12**, 073030 (2010).
[15] S. Raghu, X.-L. Qi, C.-X. Liu, D. J. Scalapino, and S.-C. Zhang, Phys. Rev. B **77**, 220503 (2008).
[16] L. Boeri, O. V. Dolgov, and A. A. Golubov, Phys. Rev. Lett. **101**, 026403 (2008).
[17] A. M. Oleś, Phys. Rev. B **28**, 327 (1983).
[18] R. Yu, K. T. Trinh, A. Moreo, M. Daghofer, J. A. Riera, S. Haas, and E. Dagotto, Phys. Rev. B **79**, 104510 (2009).
[19] S. Daul, D. J. Scalapino, and S. R. White, Phys. Rev. Lett. **84**, 4188 (2000).
[20] F. Krüger, S. Kumar, J. Zaanen, and J. van den Brink, Phys. Rev. B **79**, 054504 (2009).

[21]K. I. Kugel and D. I. Khomskii, Sov. Phys. Usp. **25**, 231 (1982).
[22]B. N. Parlett, *The Symmetric Eigenvalue Problem* (Prentice-Hall, Upper Saddle River, 1980).
[23]P. A. Lee and X.-G. Wen, Phys. Rev. B **78**, 144517 (2008).
[24]M. Daghofer, A. Nicholson, A. Moreo, and E. Dagotto, Phys. Rev. B **81**, 014511 (2010).
[25]Notice that, while this symmetry does not apply to the 122 pnictides and chalcogenides, it is still used for these materials both by theorists [T. A. Maier, S. Graser, P. J. Hirschfeld, and D. J. Scalapino, Phys. Rev. B **83**, 100515(R) (2011); T. Saito *et al.*, *ibid.* **83**, 140512(R) (2011)] and by experimentalists to report ARPES results [Lin Zhao *et al.*, Phys. Rev. B **83**, 140508(R) (2011)].
[26]Y. Gao, W.-P. Su, and J.-X. Zhu, Phys. Rev. B **81**, 104504 (2010).
[27]At $J_H/U = 0.3(0.1)$ the phase diagram Fig. 3(b) was found to be qualitatively similar to the case of $J_H/U = 0.2$ except that the "no binding" region shrinks (expands) in size.
[28]Q. Luo, G. B. Martins, D.-X. Yao, M. Daghofer, R. Yu, A. Moreo, and E. Dagotto, Phys. Rev. B **82**, 104508 (2010).
[29]J. J. Ying *et al.*, Phys. Rev. Lett. **107**, 067001 (2011).
[30]H. Ikeda, R. Arita, and J. Kuneš, Phys. Rev. B **81**, 054502 (2010).
[31]E. Dagotto, J. Riera, and A. P. Young, Phys. Rev. B **42**, 2347 (1990).
[32]K. Suzuki, H. Usui, and K. Kuroki, Phys. Rev. B **84**, 144514 (2011).
[33]R. Arita and H. Ikeda, J. Phys. Soc. Jpn. **78**, 113707 (2009).
[34]C. Platt, R. Thomale, and W. Hanke, Phys. Rev. B **84**, 235121 (2011).